
This is an electronic reprint of the original article.
This reprint may differ from the original in pagination and typographic detail.

Emadi, F.; Vuorinen, V.; Ross, G.; Paulasto-Kröckel, M.

Co, In, and Co–In alloyed Cu_6Sn_5 interconnects: Microstructural and mechanical characteristics

Published in:
Materials Science and Engineering: A

DOI:
[10.1016/j.msea.2023.145398](https://doi.org/10.1016/j.msea.2023.145398)

Published: 10/08/2023

Document Version
Publisher's PDF, also known as Version of record

Published under the following license:
CC BY

Please cite the original version:
Emadi, F., Vuorinen, V., Ross, G., & Paulasto-Kröckel, M. (2023). Co, In, and Co–In alloyed Cu_6Sn_5 interconnects: Microstructural and mechanical characteristics. *Materials Science and Engineering: A*, 881, Article 145398. <https://doi.org/10.1016/j.msea.2023.145398>

This material is protected by copyright and other intellectual property rights, and duplication or sale of all or part of any of the repository collections is not permitted, except that material may be duplicated by you for your research use or educational purposes in electronic or print form. You must obtain permission for any other use. Electronic or print copies may not be offered, whether for sale or otherwise to anyone who is not an authorised user.



Co, In, and Co–In alloyed Cu_6Sn_5 interconnects: Microstructural and mechanical characteristics

F. Emadi^{*}, V. Vuorinen, G. Ross, M. Paulasto-Kröckel

Department of Electrical Engineering and Automation, School of Electrical Engineering, Aalto University, PO Box 13340, FI-00076, Aalto, Finland

ARTICLE INFO

Keywords:

Cu–Sn interconnects
 Cu_6Sn_5 IMC
 Solid liquid interdiffusion bonding
 Mechanical reliability
 3D integration
 Soldering

ABSTRACT

The mechanical reliability of the future miniaturized interconnects is mainly governed by the intermetallic compounds such as Cu_6Sn_5 . Alloyed Cu_6Sn_5 with various elements, including Co and In, have been introduced and attracted attention for different reasons, such as the enhancing mechanical reliability and lowering the bonding temperature. Hence, this work aimed to evaluate the microstructural and mechanical properties of Cu_6Sn_5 , $\text{Cu}_6(\text{Sn},\text{In})_5$, $(\text{Cu},\text{Co})_6\text{Sn}_5$, and $(\text{Cu},\text{Co})_6(\text{Sn},\text{In})_5$ -interconnects. The grain size, grain orientation, and crystal structure of the pure and alloyed Cu_6Sn_5 phases were analyzed using electron backscatter diffraction. The results revealed that all the joints contained monoclinic and hexagonal crystal structures arbitrarily formed across the bond-line. Furthermore, the Cu_6Sn_5 grains exhibited random grain orientation and there was no discernible difference between the pure and alloyed Cu_6Sn_5 interconnects other than $\text{Cu}_6(\text{Sn},\text{In})_5$ grains elongated along the perpendicular direction to the bonding interface. However, it was found that alloying elements altered the grain sizes. In alloying refined and elongated the Cu_6Sn_5 grains while the Co alloying enlarged the Cu_6Sn_5 grains. The mechanical properties of the interconnects were examined using nanoindentation test. The results indicated that the hardness (H) and Young's modulus (E_i) values of Cu_6Sn_5 is increased with the alloying elements. $(\text{Cu},\text{Co})_6(\text{Sn},\text{In})_5$ showed the highest E_i/H value which indicates its highest plasticity.

1. Introduction

Recently, three-dimensional (3D) integration, wafer stacking or chips with vertical interconnections, has been developed to overcome the electronic components scaling limits [1–3]. To meet the demand for higher integration, miniaturized fine pitch interconnections are necessary. Smaller interconnects would, however, result in a higher volume proportion of intrinsically brittle intermetallic compounds (IMCs) in 3D micro-joints, such as those produced by the Solid Liquid Interdiffusion (SLID) bonding method [1,4,5]. If the bumps size is less than 10 μm , the entire micro-joint might only consist of a few IMCs grains [4,5]. Therefore, micro-joint reliability in future electronic packages are greatly influenced by the characteristics of the IMCs formed in the bond-line [4,6]. Understanding the microstructural and mechanical properties of these IMCs is of utmost importance, as they directly influence the reliability, durability, and performance of micro-joints. By delving into the microstructural characteristics, crystal structure, grain orientation, and mechanical behavior of these IMCs, we can gain valuable insights into their response to external stresses and uncover

strategies to enhance the mechanical reliability of future micro-joints.

Cu_6Sn_5 and Cu_3Sn are the main IMCs formed in the Sn-based solders/Cu interconnects [7]. Cu_6Sn_5 based joints are potentially thermo-mechanically more superior compared to Cu_3Sn based joints due to reliability challenging Kirkendall void formation and growth associated with Cu_3Sn formation. Therefore, intensive research [8–11] has been conducted to stabilize Cu_6Sn_5 and inhibit the formation of Cu_3Sn . For example, the addition of Co to the Cu–Sn system stabilizes the Cu_6Sn_5 phase while preventing the formation of Cu_3Sn [12–14]. Nonetheless, Cu–Sn IMC joints are often unsuitable for temperature sensitive components due to their high bonding temperature ($T > 250\text{ }^\circ\text{C}$) [15]. Cu–Sn–In, for instance, has been demonstrated as an alternative to the Cu–Sn system by lowering the bonding temperature, stabilizing the Cu_6Sn_5 phase, and preventing the Cu_3Sn phase formation [15,16]. To effectively use Co and In as alloying elements in Cu–Sn systems, a thorough knowledge of the mechanical characteristics of pure Cu_6Sn_5 interconnects as well as the effects of the alloying elements is required.

Intensive research has been conducted to investigate the mechanical properties (Young's modulus (E_i) and hardness (H)) of the Cu_6Sn_5 IMC

^{*} Corresponding author.

E-mail address: fahimeh.emadi@aalto.fi (F. Emadi).

<https://doi.org/10.1016/j.msea.2023.145398>

Received 20 April 2023; Received in revised form 29 June 2023; Accepted 1 July 2023

Available online 3 July 2023

0921-5093/© 2023 The Authors. Published by Elsevier B.V. This is an open access article under the CC BY license (<http://creativecommons.org/licenses/by/4.0/>).

[4,17–22]. The Young's modulus and hardness values for Cu_6Sn_5 varies across sources, the results, however, can be impacted by several variables, including sample preparation, measurement methods, and measurement conditions. Moreover, the Cu_6Sn_5 has a variety of crystal structures that could each have a unique mechanical characteristic. It has been shown that Cu_6Sn_5 has at least two crystal structures in the solid state, including a hexagonal structure with space group of $P6_3/mmc$ and a monoclinic structure with space group of $C2/c$ [1,7]. However, $\text{Cu}_6\text{Sn}_5 - P6_3/mmc$ is thermodynamically expected to transform to the $\text{Cu}_6\text{Sn}_5 - C2/c$ at the temperature range below 189°C . This transformation is partially hampered because of insufficient time during the cooling down process [1]. Cu_6Sn_5 is thus observed at room temperature in both hexagonal and monoclinic crystal structures. The mechanical properties of the Cu_6Sn_5 IMC in relation to its crystal structure has been previously studied, and has been found that the hexagonal Cu_6Sn_5 has a comparable hardness to monoclinic Cu_6Sn_5 , but with a higher Young's modulus [23].

According to the literature, hexagonal- Cu_6Sn_5 shows intrinsic anisotropic mechanical properties [19,22,24]. As a result, the orientation of the Cu_6Sn_5 grain can impact the observed Young's modulus and hardness. According to V. Kumar et al., Cu_6Sn_5 formed at Sn-based solder/polycrystalline Cu pads has no preferred orientation [25]. While K. H. Prakash reported that Cu_6Sn_5 films exhibits a strong grain orientation in the directions $\langle 102 \rangle$ and $\langle 101 \rangle$. According to Y. Tian, both scallop shape and roof shape Cu_6Sn_5 has a preferred orientation of $\{001\}$ plane parallel to polycrystalline Cu surface [26]. Cu_6Sn_5 IMC can have a variety of grain orientations. Therefore, it is crucial to have a comprehensive understanding of how the mechanical properties of Cu_6Sn_5 relate to grain orientation to assess the mechanical reliability of the joint. For instance, (001) plane of hexagonal Cu_6Sn_5 has the highest elastic modulus and hardness than the other crystal planes [22,27]. The presence of even a single Cu_6Sn_5 grain with weak mechanical properties may deteriorate the reliability of future micro-joints containing a few Cu_6Sn_5 grains. Hence, a consistent mechanical response of Cu_6Sn_5 grains to the external stresses is desired [21]. However, achieving a micro-joint with constant mechanical response of Cu_6Sn_5 grains demands defined crystal structure and orientation, which complicates the fabrication process.

It is possible to assess the mechanical behavior of Cu_6Sn_5 joints in part by measuring the E_i/H value. It has been proposed that the plasticity of the intrinsic brittle materials such as Cu_6Sn_5 intermetallic compounds can be evaluated by the modulus/hardness ratio (E_i/H) [28]. According to J. Song, the critical value for E_i/H is 17.3–17.5, below which the indent morphology of Cu_6Sn_5 turns brittle [23]. Given that the brittleness of the IMCs is the main factor in IMCs micro-joints failure, Cu_6Sn_5 -based joints with higher E_i/H values are preferred. However, the minimum required E_i/H value depends on the specific application. The E_i/H ratio for Cu_6Sn_5 is calculated to be 17 and 19.5, respectively, according to F.X. Che et al. [29] and V. Marques [30]. Nevertheless, when third elements are added to Cu–Sn systems, they can take part in the Cu_6Sn_5 formation and alter its mechanical properties. As a result, when examining Cu_6Sn_5 's characteristics, the additive elements must be considered.

The effects of third elements such as Ni and Zn on the microstructural and mechanical characteristics of Cu_6Sn_5 have been investigated [31–38]. However, there is insufficient data on how cobalt and indium affect the mechanical and microstructural characteristics of Cu_6Sn_5 . Grain refinement has been observed by dissolution of Co in the Cu_6Sn_5 IMC, while Co does not alter the Cu_6Sn_5 grain morphology [39,40]. Furthermore, it has been found that Co and In additive stabilizes the hexagonal- Cu_6Sn_5 down to room temperature [15,41]. A. Yang et al. [11] reported that indium alloying element change the microstructure of the Cu_6Sn_5 IMC as follows: a) refining the grains and b) increasing the crystal cell volume. The Young's modulus of Cu_6Sn_5 with a small amount of indium ($\text{Cu}_{54.8}\text{Sn}_{38.5}\text{In}_{6.7}$) was measured to be 102.48 GPa [42]. According to W. Huang [43], the Young's modulus of Cu_6Sn_5 increase by In

alloying while A. Luktuke et al. [44] reported to the contrary (a decrease in Cu_6Sn_5 Young's modulus by In alloying). In our previous work, we have briefly studied the mechanical and microstructural properties of Cu_6Sn_5 formed in the Cu–Sn, Cu–Sn–Co, Cu–Sn–In, and Cu–Sn–In–Co SLID systems [13,14,16,45]. However, there is no comprehensive study on both microstructural and mechanical properties of the Cu_6Sn_5 IMC alloyed by Co and In. Hence, in this study we aimed to investigate the impact of third element, Co, In, and Co/In, elements on the microstructural and mechanical properties of the low-temperature Cu–Sn–based SLID joints primarily composed of Cu_6Sn_5 phase. The crystal structure, grain size and grain orientation of the Cu_6Sn_5 , $\text{Cu}_6(\text{Sn},\text{In})_5$, $(\text{Cu},\text{Co})_6\text{Sn}_5$, and $(\text{Cu},\text{Co})_6(\text{Sn},\text{In})_5$ joints were characterized using EBSD technique. Furthermore, the mechanical properties (E_i and H) of the abovementioned joints were measured using nanoindentation.

2. Materials and methods

2.1. Specimen preparation

All samples were prepared on thermally oxidized (300 nm SiO_2) 100 mm Si(100) wafers. The device and cap chips for various systems (Cu–Sn, Cu–Sn–In–Cu, Cu–Sn–Co, and Cu–Sn–In–Co) were prepared as

Table 1
The fabrication process for device and cap chips in different SLID systems.

System	Fabrication process	Bonding condition
Cu–Sn–Cu	Cap and Device chips: A 60 nm thick TiW adhesion layer was sputtered on the Si wafer, and it was followed by a 100 nm thick copper seed layer sputtering. 4 μm of copper was electroplated utilizing NB Semi plate Cu 100 bath, followed by 2 μm of the electroplated tin using NB Semi plate Sn 100 solution from NB technologies. Then the wafer was cut into 1^*1 cm pieces.	250 $^\circ\text{C}$, 0.5 h
Cu–Sn–Co	Cap chip: A 60 nm thick TiW adhesion layer was sputtered on the Si wafer, and it was followed by a 100 nm thick copper seed layer sputtering. 4 μm of copper was electroplated utilizing NB Semi plate Cu 100 bath, followed by 2 μm of the electroplated tin using NB Semi plate Sn 100 solution from NB technologies. Then the wafer was cut into 1^*1 cm pieces. Device chip: A 60 nm thick Ti adhesion layer was sputtered on the Si wafer, and it was followed by a 200 nm thick Mo barrier layer and 80 nm Co sputtering. The wafer was diced into 1^*1 cm pieces.	250 $^\circ\text{C}$, 1 h
Cu–Sn–In–Cu	Cap and Device chips: A 60 nm thick TiW adhesion layer was sputtered on the Si wafer, and it was followed by a 100 nm thick copper seed layer sputtering. 5 μm of copper was electroplated utilizing NB Semi plate Cu 100 bath, followed by 1.7 μm of the electroplated tin using NB Semi plate Sn 100 solution from NB technologies and 1.7 μm of the electroplated indium using indium sulfamate plating bath. Finally, the wafer was cut into 1^*1 cm pieces.	200 $^\circ\text{C}$, 1 h
Cu–Sn–In–Co	Cap chip: A 60 nm thick TiW adhesion layer was sputtered on the Si wafer, and it was followed by a 100 nm thick copper seed layer sputtering. 5 μm of copper was electroplated utilizing NB Semi plate Cu 100 bath, followed by 1.7 μm of the electroplated tin using NB Semi plate Sn 100 solution from NB technologies and 1.7 μm of the electroplated indium using indium sulfamate plating bath. The wafer was cut into 1^*1 cm pieces. Device chip: Co foil (purity: 99.99%, Goodfellow Ltd.) 1 mm in thickness was cut into pieces 1^*1 cm in size. The pieces were mechanically ground to 2400 papers, cleaned with acetone, and air-dried before bonding.	200 $^\circ\text{C}$, 1 h

described in Table 1. They were then soldered in an air muffle furnace. Because Sn–In has a lower melting point than Sn, samples with Sn and In were bonded at a lower bonding temperature (200 °C) than those with just Sn ($T_b = 250$ °C). Fig. 1 shows a schematic illustration of the process flow for Cu–Sn sample (as an example).

2.2. EBSD measurements

EBSD maps were collected using a scanning electron microscope equipped with electron backscatter diffraction (EBSD) (JIB-4700F). For cross-section analysis using EBSD, samples were prepared in three steps: 1) using standard metallographic methods, 2) chemical etching in a solution with hydrochloric acid and nitric acid diluted in distilled water, and 3) ion beam polishing using JEOL Ion Beam Cryo Cross Section Polisher with ion beam accelerating voltage of 4 kV for 5 min. The EBSD analysis was carried out in the bond-line and focused on the Cu_6Sn_5 IMC using SEM/EDX analysis prior to the EBSD measurements. The following EBSD detector settings were used during the EBSD data acquisition: 70° sample tilt; 20 kV accelerating voltage; 14 nA probe current; 10 mm working distance; and 20 nm EBSD step size. The lattice parameters of the phases used for the EBSD data collection are summarized in Table 2. The band contrast map, phase color map, inverse pole figure Y color map, and (001) pole figures of both monoclinic and hexagonal Cu_6Sn_5 were collected using AZtecCrystal EBSD Processing Software. In this paper, the cross-section surface perpendicular was the normal direction (ND). The transvers direction (TD) and rolling direction (RD) were along the joint cross-section surface and TD was parallel to the bond-line.

2.3. Mechanical properties characterization

Nano-indentation test was performed within the IMC layers at the joint area of Cu–Sn, Cu–Sn–In, Cu–Sn–Co, and Cu–Sn–In/Co stacks using a CSM Instruments Nanoindentation tester. A Berkovich diamond indenter was used with following load function parameters: 5 mN maximum load, 10 mN/min loading and unloading rate, and 15 s hold time. The samples were measured using the continuous data of the applied load (P) and indenter displacement (h) during the test. The

Table 2
Lattice parameters of the phases used for EBSD data collection.

Phase	a	b	c	Alpha	Beta	Gamma
Cu	3.62	3.62	3.62	90	90	90
Hexagonal- Cu_6Sn_5	4.19	4.19	5.04	90	90	120
Monoclinic- Cu_6Sn_5	11.2	7.28	9.83	90	98.84	90
Cu_3Sn	6.12	6.12	6.12	90	90	90

phase composition of the indentation marks was analyzed using a JSM-6330F field emission scanning electron microscope (SEM; JEOL Ltd.) and INCA X-sight energy-dispersive X-ray spectroscopy (EDX) system (Oxford Instruments). The mechanical characteristics analysis was done using the data for the indents within the Cu_6Sn_5 phase. For example, Fig. 2 shows the BSE-EDX micrograph of the indents on the Cu–Sn–Co

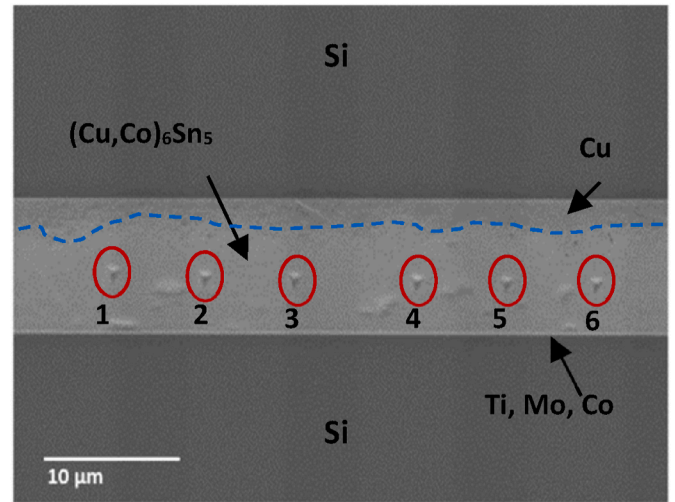


Fig. 2. BSE-SEM image of the indents on Cu–Sn–Co joint bonded at 250 °C for 1h

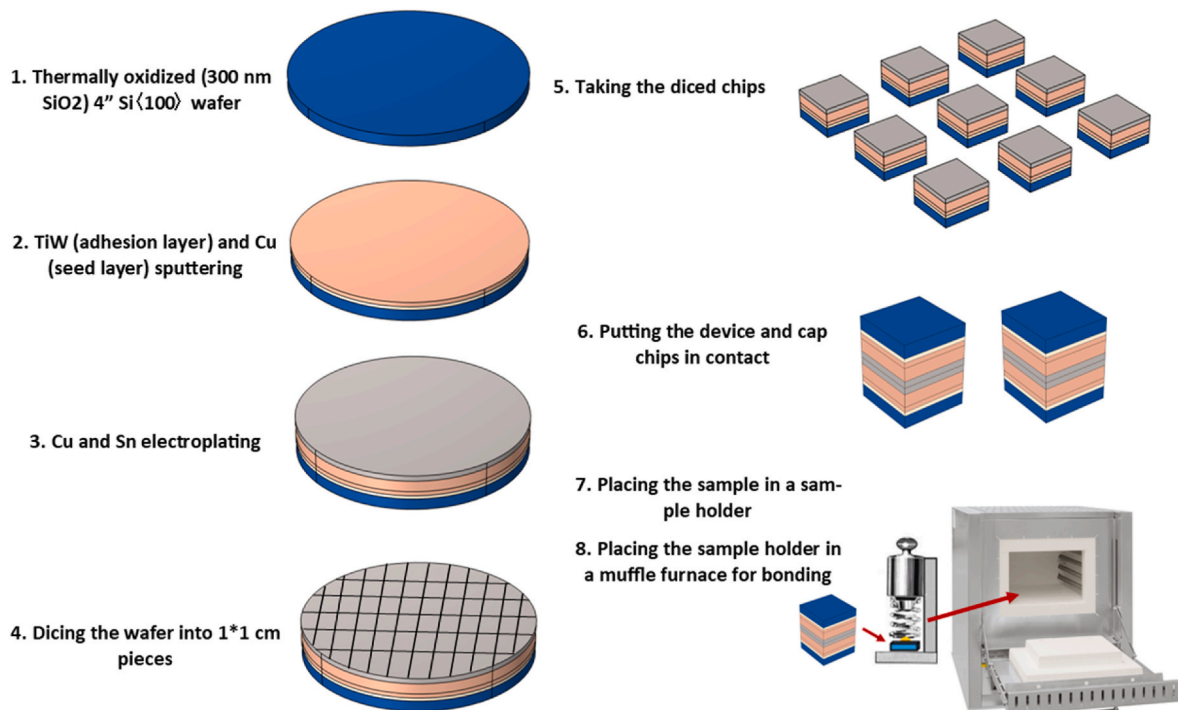


Fig. 1. A schematic illustration of fabrication process of the Cu–Sn SLID bonded sample as an example.

joint bonded at 250 °C for 1 h. The continuous data of the indents 1 to 6 located over the $(\text{Cu},\text{Co})_6\text{Sn}_5$ phase were used to determine the mechanical properties of $(\text{Cu},\text{Co})_6\text{Sn}_5$. The Nano-Indentation hardness (H), reduced elastic modulus (E_r), and Young's modulus were calculated using equations (1)–(3), respectively.

$$H = \frac{P}{A} \quad (1)$$

$$E_r = \frac{1}{2} \frac{\sqrt{\pi}}{\sqrt{A}} \frac{dP}{dh} \quad (2)$$

$$E_r = \left(\frac{1 - \nu_s^2}{E_s} + \frac{1 - \nu_i^2}{E_i} \right) \quad (3)$$

Where P, A, and dP/dh signify the maximum indentation load, the projected area, and the onset slope of the unloading curve, respectively. And ν_i and E_i are the Poisson coefficient and the elastic properties of the diamond indenter, respectively, and ν_s is the Poisson coefficient of the measured phase. For a diamond tip, $E_i = 1140$ GPa and $\nu_i = 0.07$. And ν_s was assumed to be 0.309 for Cu_6Sn_5 phase with and without alloying elements (Co, In, and Co/In).

3. Results & discussion

3.1. EBSD measurements and analysis

Fig. 3 gives the BC (Band Contrast), phase color, and IPF-Y (Inverse Pole Figure Y) maps measured from the cross-sectional surfaces of the Cu–Sn, Cu–Sn–In, Cu–Sn–Co, and Cu–Sn–In–Co joints. All the phases across the bond-line were identified using SEM-EDX analyzing, and the Cu_6Sn_5 -containing region is indicated by the dashed-lines in Fig. 3. The results of the Band Contrast maps (Fig. 3 a-d) reveal that the different alloying elements (Co and In) have a distinct impact on the Cu_6Sn_5 morphology. By adding In into Cu_6Sn_5 interconnects, the grains are refined and elongated in RD. While the addition of Co as an alloying element increased the size of Cu_6Sn_5 grains. The average grain size (both width and length of the grains) of Cu_6Sn_5 , $\text{Cu}_6(\text{Sn},\text{In})_5$, $(\text{Cu},\text{Co})_6\text{Sn}_5$, and $(\text{Cu},\text{Co})_6(\text{Sn},\text{In})_5$ interconnects calculated using BC maps is shown in Fig. 4. The $(\text{Cu},\text{Co})_6\text{Sn}_5$ showed the largest average grain size. $\text{Cu}_6(\text{Sn},\text{In})_5$ on the other hand, had grains with smallest size. In general, the alloying elements involved in phase (such as Cu_6Sn_5) formation lower the critical nucleus energy, which enhances the nucleus and may subsequently refine the grain sizes [46]. However, according to Y. Wang et al. Co (which occupy the Cu site [47]) promotes the Cu_6Sn_5 IMC

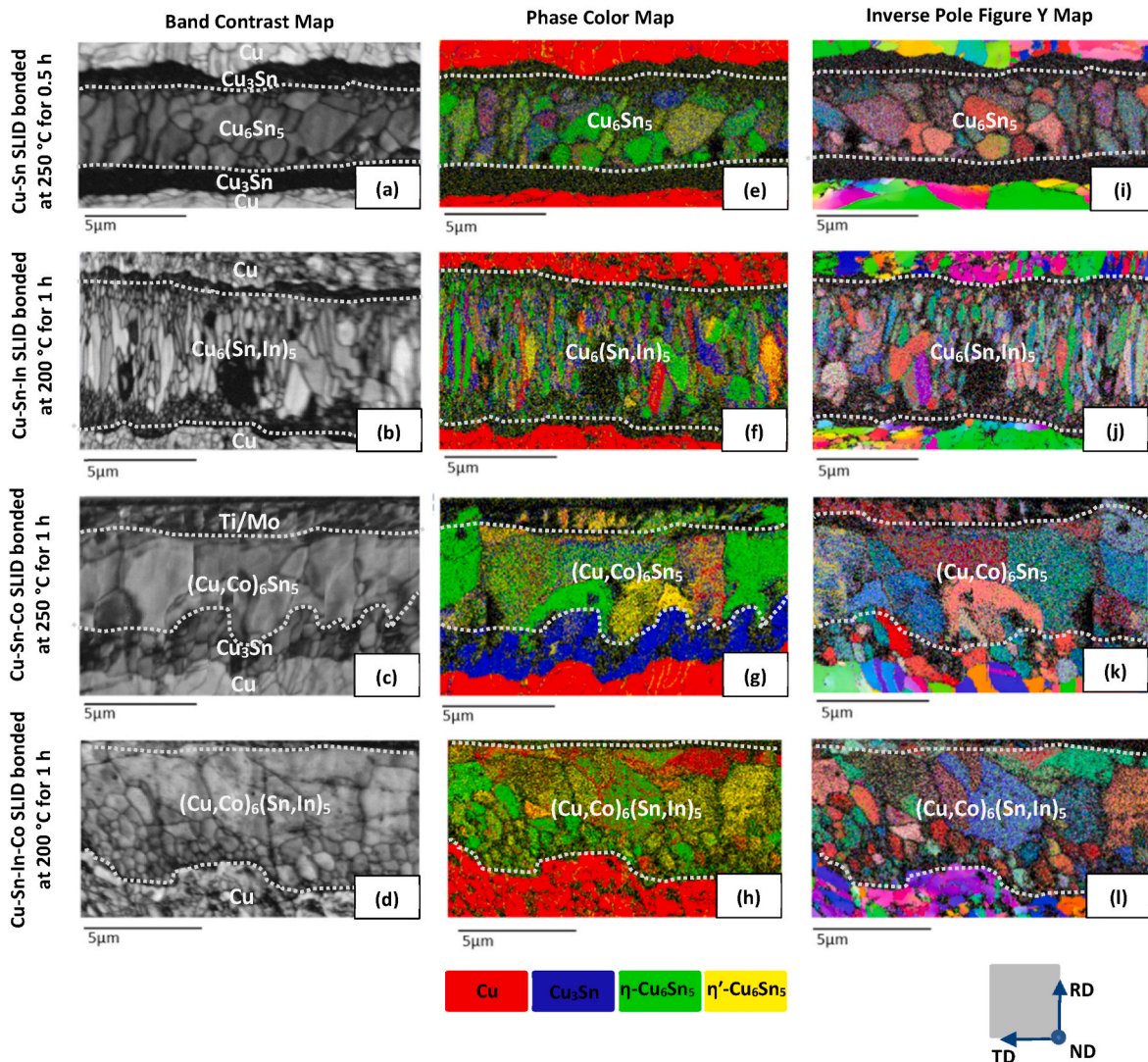


Fig. 3. EBSD analysis of cross-sectional grain structures of Cu–Sn-base SLID systems, Band Contrast Map: (a) Cu–Sn, (b) Cu–Sn–In, (c) Cu–Sn–Co, and (d) Cu–Sn–In–Co SLID bonded samples; (e–h) the corresponding Phase Color Maps; and (i–l) the corresponding Inverse Pole Figure X color maps. (For interpretation of the references to color in this figure legend, the reader is referred to the Web version of this article.)

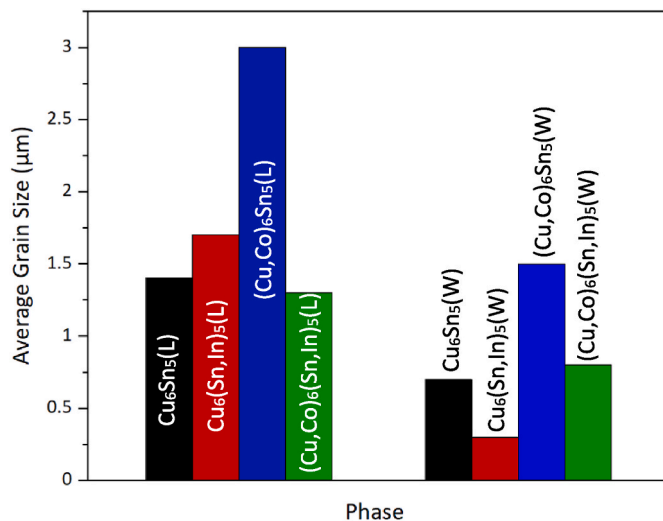


Fig. 4. The average grain size (width and length of the grains) of Cu₆Sn₅ phase formed in Cu-Sn, Cu-Sn-In, Cu-Sn-Co, and Cu-Sn-In-Co joints.

growth kinetics by decreasing the atomic diffusion energy of Cu along [201] direction. On the other hand, In (which occupy the Sn site) shows the opposite impact on the atomic diffusion energy of Cu along [201] direction and the corresponding Cu₆Sn₅ IMC growth kinetics [11,47]. In the current work, the Cu-Sn-In and Cu-Sn-Co joints were bonded at a temperature of 80° and 20° above the melting point of (Sn-In) and Sn, respectively. Hence, Cu₆(Sn,In)₅ grains (formed in Cu-Sn-In) were expected to grow to a larger size than (Cu,Co)₆Sn₅ grains (formed in Cu-Sn-Co) assuming there are no differences in the growth kinetic parameters of Cu₆(Sn,In)₅ and (Cu,Co)₆Sn₅ grains. Therefore, the opposing observations may indicate that Co and In have different effects on the growth kinetics of Cu₆Sn₅, promoting and decreasing, respectively. The Cu₆Sn₅ grain size varied across the Cu-Sn-In-Co bond-line, with larger grains forming near the Co side and smaller grains forming close to the Cu side. It can plausibly be due to the differing Co content in the Cu- and Co-side's grains, (Cu,Co)₆(Sn,In)₅ grains with highest Co content nucleated and grown in the Co-side [13,14,45]. As a result, the Co/In co-alloying does not exhibit consistent effect on the size of Cu₆Sn₅ grains and is drastically changed by Co content, lower Co content results in smaller grains and higher Co content results in bigger grains. (Cu,Co)₆(Sn,In)₅ with higher Co content displays roughly the same grain shape and size as (Cu,Co)₆Sn₅. However, with less Co, (Cu,Co)₆(Sn,In)₅ exhibits completely different grain morphology and size, as they are considerably smaller and more rounded.

Fig. 3i-l show the phase color maps for the four different joints. The Cu, Cu₃Sn and hexagonal and monoclinic crystal structures of Cu₆Sn₅ are shown in red, blue, green, and yellow, respectively. The hexagonal and monoclinic-Cu₆Sn₅ were randomly distributed across the bond-line. A small portion of the region that was identified by SEM/EDX as Cu₆Sn₅ was incorrectly recognized by EBSD analysis as Cu and Cu₃Sn. It is plausible that the discrepancy is attributed to poor data and diffraction patterns obtained from those specific regions of the samples. This issue is probably caused by the challenging sample preparation process for such samples due to several reasons. These include the narrow bond-line (under 10 μm) with small grains, and complex crystal structures of IMCs which requires better surface quality.

Additionally, there was no clear difference between the preferred crystal structure of Cu₆Sn₅ formed in the pure Cu-Sn SLID joint and the alloyed Cu-Sn SLID systems. The proportion of hexagonal and monoclinic Cu₆Sn₅ determined for each joint are listed in Table 3. Cu₆Sn₅, Cu₆(Sn,In)₅, (Cu,Co)₆(Sn,In)₅, and (Cu,Co)₆(Sn,In)₅ interconnects all has hexagonal to monoclinic ratio of approximately 0.5–0.6, while (Cu,Co)₆Sn₅ interconnects has a ratio of about 1. However, it was expected to

Table 3

The percentage of Hexagonal and Monoclinic Cu₆Sn₅ in the studied joints.

	Cu-Sn SLID bonded at 250 °C for 1 h	Cu-Sn-In SLID bonded at 200 °C for 1 h	Cu-Sn-Co SLID bonded at 250 °C for 1 h	Cu-Sn-In-Co SLID bonded at 200 °C for 1 h
Hexagonal (%)	37	38	49	34
Monoclinic (%)	63	62	51	66

have only hexagonal-Cu₆Sn₅ by Co and In alloying. According to the literature [48], the Cu₆Sn₅ formed in Cu-Sn system comprises of both monoclinic and hexagonal crystal structures due to the inadequate transferring time for hexagonal to monoclinic, however, the monoclinic Cu₆Sn₅ is the thermodynamic stable phase at room temperature. Nevertheless, upon long-term annealing at 150 °C, the Cu₆Sn₅ hexagonal will entirely transform to the monoclinic crystal structure. According to the findings of the current work, the same phenomenon exists for Cu₆Sn₅ with either Co, In, or Co/In alloying elements, displaying both hexagonal and monoclinic crystal forms at ambient temperature. However, further investigation is needed to determine how the aging affect the crystal structure transformation for the Cu₆Sn₅ phase alloyed with Co, In, or Co/In.

The inverse pole figure (IPF) maps are presented in Fig. 3 i-l. The IPF maps reveal that Cu₆Sn₅ grains have varying orientation with no preferential orientation. To confirm the Cu₆Sn₅ orientation distribution observed in IPF maps, hexagonal and monoclinic (001) pole figures of the Cu₆Sn₅, Cu₆(Sn,In)₅, (Cu,Co)₆Sn₅, and (Cu,Co)₆(Sn,In)₅ IMCs were investigated (Fig. 5). According to the pole figures, the Cu₆Sn₅ grains formed in the Cu-Sn, Cu-Sn-Co, and Cu-Sn-In-Co SLID systems exhibited a random orientation distribution. However, the poles of Cu₆(Sn,In)₅ formed in Cu-Sn-In system was mostly aligned with the RD and the C-direction of the hexagonal and monoclinic Cu₆Sn₅ was parallel to the RD. This is also clearly visible on the correlated IPF map (Fig. 3-j), the grains are mostly columnar and elongate in RD direction.

In general, the grain orientation diversification and fine grains strengthen the mechanical properties and improve the mechanical reliability of the joints due to hindering a direct stress propagation to adjacent crystal planes and grain boundary strengthening mechanism. The diversification of the grain orientation, however, could result in the failure of some bumps and possibly the entire joint in the future microbumps, where each interconnection would contain only a few Cu₆Sn₅ grains. Since a bump only consists of a small number of randomly oriented Cu₆Sn₅ grains, if one of the grains is oriented so that its mechanical characteristics are poor, it can significantly impact the mechanical properties of the entire joint. Therefore, engineering the grain orientation for extremely small bumps or to refining the grain size such that there is enough variety in the grain orientation might be beneficial.

3.2. Mechanical characterization

Representative nanoindentation load-displacement curves during the indentation on Cu₆Sn₅, Cu₆(Sn,In)₅, (Cu,Co)₆Sn₅, and (Cu,Co)₆(Sn,In)₅ interconnects are shown in Fig. 6. The corresponding measured hardness (H), elastic modulus (Er), Young's modulus (Ei), and Ei/H are listed in Table 4. For the Cu₆Sn₅ interconnects the Young's modulus and hardness are measured to be 113.6 ± 1.1 and 6.7 ± 0.5 GPa. The average values of Cu₆Sn₅ are in good agreement with previously reported values [1,6,49–52]. Both the elastic modulus and hardness of (Cu,Co)₆Sn₅ and Cu₆(Sn,In)₅ interconnects are greater than their corresponding values for Cu₆Sn₅ interconnects. However, the co-alloying of Co and In into Cu₆Sn₅ exhibited a different impact on the mechanical properties of the Cu₆Sn₅ interconnects compared to the single Co or In

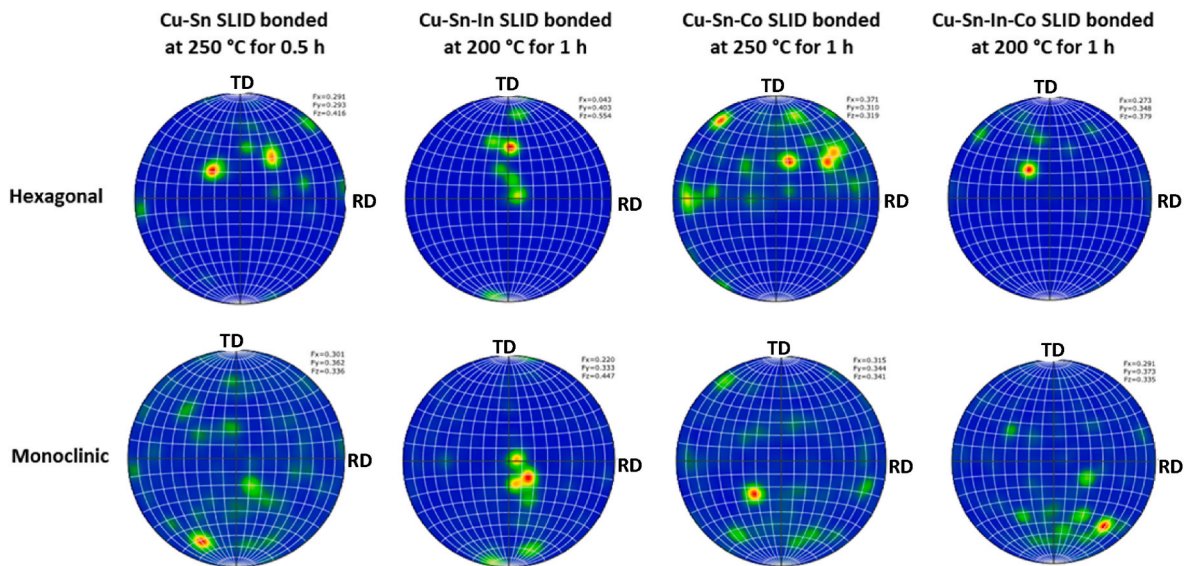


Fig. 5. EBSD pole figures of both hexagonal and monoclinic Cu_6Sn_5 IMC in Cu–Sn, Cu–Sn–In, Cu–Sn–Co, and Cu–Sn–In–Co bond at 250 °C, 0.5 h, 200 °C, 1 h, 250 °C, 1 h, and 200 °C, 1 h, respectively.

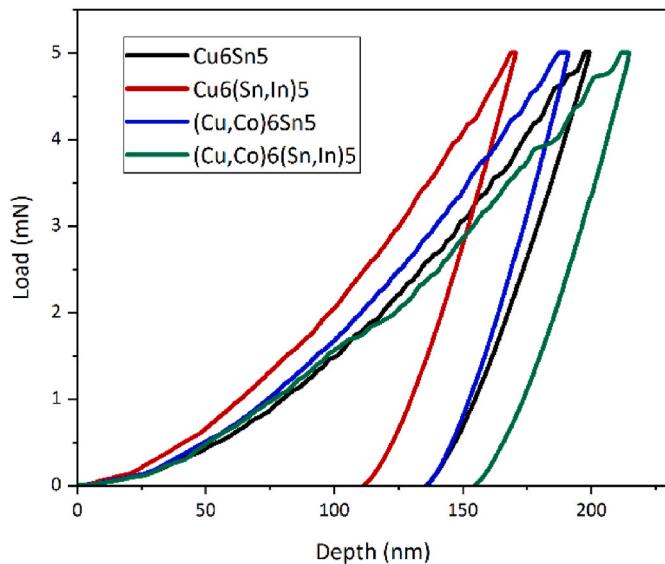


Fig. 6. Representative load–displacement curves from nanoindentation lateral to IMC layers.

Table 4
The mechanical properties of the IMCs.

	$(\text{Cu,Co})_6(\text{Sn, In})_5$	$\text{Cu}_6(\text{Sn, In})_5$	$(\text{Cu, Co})_6\text{Sn}_5$	Cu_6Sn_5
Hardness (H) (GPa)	5.7 ± 1	9.1 ± 1	6.9 ± 0.2	6.7 ± 0.5
Reduced elastic modulus (Er) (GPa)	106.9 ± 11	132.6 ± 5.5	122 ± 6	103.3 ± 0.9
Young's modulus (Ei) (GPa)	118 ± 14	150 ± 7	136 ± 8	113.6 ± 1.1
Ei/H	20.7 ± 0.9	16.4 ± 2.3	19.7 ± 1.4	17.0 ± 0.8
Cu (at%)	51.9 ± 3	52.1 ± 3.5	51.7 ± 3.3	55.3 ± 3
Co (at%)	3.7 ± 1.6	0	2.1 ± 1	0
Sn (at%)	19.6 ± 5.7	26.8 ± 2	45.9 ± 1.6	44.7 ± 2
In (at%)	24.8 ± 3.7	21.1 ± 3.3	0	0

alloying elements, the hardness decreased, whereas the Young's modulus increased slightly. Compared to Cu_6Sn_5 interconnect, the alloyed Cu_6Sn_5 interconnects had larger scatter in hardness and Young's modulus values and $(\text{Cu,Co})_6(\text{Sn,In})_5$ interconnect showed the highest scatter in the Young's modulus values measured from various locations along the bond line.

The different mechanical properties of Cu_6Sn_5 interconnects listed in Table 4 as well as the scatter of Young's modulus and hardness values may be caused by several factors. These factors include changes in the crystal structure of the Cu_6Sn_5 from one sample to another or from one analyzed point to another, different growth texture for each joint and anisotropy in the mechanical properties, and the chemical composition and the grain size change by alloying elements (Co, In, and Co/In) [19, 53]. For instance, it has been shown that the hexagonal- Cu_6Sn_5 has higher Ei and H values than monoclinic- Cu_6Sn_5 [54]. Additionally, it has been previously claimed that the mechanical properties of the Cu_6Sn_5 is strongly anisotropic and related to the crystal orientation [22] and alloying elements. For instance, according to S. Mu et al., the average values and standard deviations in both elastic modulus and hardness for $(\text{Cu,Ni})_6\text{Sn}_5$ are higher than Cu_6Sn_5 due to the growth of the preferred (101) texture and the anisotropy in mechanical properties of $(\text{Cu, Ni})_6\text{Sn}_5$ [19]. In addition, the IMCs' mechanical characteristics can be impacted by grain size, Young's modulus increases with increasing grain size. However, the grain size has a considerable impact on the mechanical properties of materials when the grains size is in the nanoscale [55–57].

It was determined from the EBSD analyses of the various samples that all of the interconnects contained hexagonal and monoclinic Cu_6Sn_5 , randomly distributed across the bond-line. Furthermore, it was observed that the Cu_6Sn_5 in four studied joints exhibited randomly orientated polycrystalline grains (however, the $\text{Cu}_6(\text{Sn,In})_5$ shows grains with c-axis elongated in the RD direction). As a result, it is difficult to correlate the crystal structure and grain orientation of various joints, which could account for their varying mechanical properties. However, the varying mechanical properties for different joints and analyzed sites in each joint may be explained by the chemical composition change from one joint to another or across the bond-line. The chemical composition change by the alloying elements can lead to the solid solution strengthening. For instance, it has been claimed that Ni substitution with Cu in Cu_6Sn_5 lattice reduces the Cu_6Sn_5 unit cell volumes, generates inter-atomic stresses around the Ni atoms, and subsequently increases Young's modulus and hardness [22,58]. Therefore, the same

phenomenon might occur when Cu_6Sn_5 is alloyed with Co and In. As mentioned, Cu and Sn atoms in Cu_6Sn_5 would be replaced by Co and In, respectively. Co, Cu, In, and Sn all have distinct atomic radii, hence any substitutions would result in substitutional defects. Additionally, Co–Sn and Cu–In interact more strongly than Cu–Sn based on their binary phase diagram. Therefore, by adding Co or In alloying elements into Cu_6Sn_5 , the Young's modulus and hardness values may increase because of these effects (substitutional defects and greater atoms interaction). It is crucial to note that, in the current study, approximately 50% of the Sn atoms were substituted by In in Cu–Sn–In, while in Cu–Sn–Co a small number of Cu atoms were substituted by Co atoms. Therefore, the substitutional defects impact in the studied Cu–Sn–In could be significantly higher than in the Cu–Sn–Co. Hence, it could be the reason why indium alloying showed greater impacts on the increasing of the hardness than Co alloying. However, Cu_6Sn_5 with co-alloying cobalt and indium showed completely different results, its hardness was less than while its Young's modulus was comparable to Cu_6Sn_5 . To find the impact of the co-alloying Co and In on the Cu_6Sn_5 lattice, first-principles calculations of structural and mechanical properties of Cu_6Sn_5 with Co and In is required as we have various bonds: Cu–Sn, Co–Sn, Cu–In, and Co–In.

As listed in Table 4, the E_i/H value for Cu_6Sn_5 , $\text{Cu}_6(\text{Sn},\text{In})_5$, $(\text{Cu},\text{Co})_6\text{Sn}_5$, and $(\text{Cu},\text{Co})_6(\text{Sn},\text{In})_5$ interconnects were measured to be 17.0 ± 0.8 , 16.4 ± 2.3 , 19.7 ± 1.4 , and 20.7 ± 0.9 . The $(\text{Cu},\text{Co})_6(\text{Sn},\text{In})_5$ interconnect has the greatest E_i/H value, and accordingly highest plasticity which is preferable for interconnects.

4. Conclusion

The microstructural and mechanical properties of pure and Co, In, and Co–In alloyed Cu_6Sn_5 -interconnects were investigated using EBSD and nanoindentation. The following conclusions can be drawn from this study:

1. The morphology of Cu_6Sn_5 interconnects can be modified by Co and In addition. Among the interconnects, Co containing Cu_6Sn_5 and In containing Cu_6Sn_5 have the largest and smallest average grain sizes, respectively. Notably, the grain size and morphology of $(\text{Cu},\text{Co})_6(\text{Sn},\text{In})_5$ interconnect vary across the bond-line due to fluctuations in Co content. Higher Co content corresponds to larger grains.
2. Cu_6Sn_5 , $\text{Cu}_6(\text{Sn},\text{In})_5$, $(\text{Cu},\text{Co})_6\text{Sn}_5$, and $(\text{Cu},\text{Co})_6(\text{Sn},\text{In})_5$ all exhibit both hexagonal (H) and monoclinic (M) crystal structures. Cu_6Sn_5 grains formed in all interconnects showed a random orientation distribution. However, $\text{Cu}_6(\text{Sn},\text{In})_5$ grains in the Cu–Sn–In system were mostly aligned with C-direction of the hexagonal and monoclinic Cu_6Sn_5 grains.
3. The addition of Co and In into Cu_6Sn_5 interconnects alters their mechanical properties. Incorporating Co or In reduces the Young's modulus (E_i) and hardness (H). However, co-alloying Co and In in Cu_6Sn_5 leads to decreased hardness but a slight increase in Young's modulus. The E_i/H value for Cu_6Sn_5 , $\text{Cu}_6(\text{Sn},\text{In})_5$, $(\text{Cu},\text{Co})_6\text{Sn}_5$, and $(\text{Cu},\text{Co})_6(\text{Sn},\text{In})_5$ interconnects are measured to be 17.0 ± 0.8 , 16.4 ± 2.3 , 19.7 ± 1.4 , and 20.7 ± 0.9 .
4. The $(\text{Cu},\text{Co})_6(\text{Sn},\text{In})_5$ interconnect has the greatest E_i/H value and accordingly highest plasticity, which is preferable for interconnects. Moreover, the $(\text{Cu},\text{Co})_6(\text{Sn},\text{In})_5$ grains morphology can be changed by changing the Co content. Therefore, it is possible to design the layout of the interconnects so that either small or large grains are present to take use of the mechanism for reinforcing grain boundaries or the consistent mechanical response of the joints, respectively. In addition, indium can lower the bonding temperature when compared to pure Sn, and Co can be employed as a contact metallization for Cu–Sn–In systems. As a result, Cu–Sn–In–Co interconnects have a lot to offer electronics integrations.

Funding

This work has been funded by iRel40. iRel40 is a European co-funded innovation project that has been granted by the ECSEL Joint Undertaking (JU) under grant agreement No 876659. The funding of the project comes from the Horizon 2020 research program and participating countries. National funding is provided by Germany, Austria, Belgium, Finland (Innovation Funding Agency, Business Finland), France, Italy, the Netherlands, Slovakia, Spain, Sweden, and Turkey.

CRediT authorship contribution statement

F. Emadi: Formal analysis, Investigation, Writing – original draft, Visualization. **V. Vuorinen:** Project administration, Conceptualization, Writing – review & editing. **G. Ross:** Writing – review & editing. **M. Paulasto-Kröckel:** Supervision, Conceptualization, Writing – review & editing.

Declaration of competing interest

The authors declare that they have no known competing financial interests or personal relationships that could have appeared to influence the work reported in this paper.

Data availability

Data will be made available on request.

Acknowledgment

We acknowledge the provision of facilities and technical support by Aalto University at Micronova nanofabrication center and OtaNano-Nanoscience Center (Aalto-NMC). The authors express their gratitude to Anton Klami for assistance with sample preparation.

ABBREVIATIONS

IMC	intermetallic compound
SLID	solid liquid interdiffusion
SEM	scanning electron microscope
EDX	X-ray spectroscopy
EBSD	electron backscatter diffraction; BIB, broad ion beam

References

- [1] Z.H. Zhang, C.W. Wei, J.J. Han, H.J. Cao, H.T. Chen, M.Y. Li, Growth evolution and formation mechanism of η - Cu_6Sn_5 whiskers on η - Cu_6Sn_5 intermetallics during room-temperature ageing, *Acta Mater.* 183 (2020) 340–349.
- [2] B. Lee, H. Jeon, K.W. Kwon, H.J. Lee, Employment of a bi-layer of Ni(P)/Cu as a diffusion barrier in a Cu/Sn/Cu bonding structure for three-dimensional interconnects, *Acta Mater.* 61 (18) (2013) 6736–6742.
- [3] Y. Qiao, X. Liu, J. Zhao, L. Wu, C. Liu, Morphology and orientation evolution of Cu_6Sn_5 grains on (001)Cu and (011)Cu single crystal substrates under temperature gradient, *J. Mater. Sci. Technol.* 95 (2021) 29–39.
- [4] J.Y. Wu, Y.S. Chiu, Y.W. Wang, C.R. Kao, Mechanical characterizations of single-crystalline (Cu, Ni) 6 Sn 5 through uniaxial micro-compression, *Mater. Sci. Eng., A* 753 (January) (2019) 22–30.
- [5] J. Feng, C. Hang, Y. Tian, C. Wang, B. Liu, Effect of electric current on grain orientation and mechanical properties of Cu–Sn intermetallic compounds joints, *J. Alloys Compd.* 753 (2018) 203–211.
- [6] P.F. Yang, Y.S. Lai, S.R. Jian, J. Chen, R.S. Chen, Nanoindentation identifications of mechanical properties of Cu_6Sn_5 , Cu_3Sn , and Ni_3Sn_4 intermetallic compounds derived by diffusion couples, *Mater. Sci. Eng., A* 485 (1–2) (2008) 305–310.
- [7] A. Leineweber, C. Wieser, W. Hügél, Cu_6Sn_5 intermetallic: reconciling composition and crystal structure, *Scripta Mater.* 183 (2020) 66–70.
- [8] T. Laurila, V. Vuorinen, J.K. Kivilahti, Interfacial reactions between lead-free solders and common base materials, *Mater. Sci. Eng. R Rep.* 49 (1–2) (Mar. 2005) 1–60.
- [9] S.U. Mehreen, K. Nogita, S.D. McDonald, H. Yasuda, D.H. StJohn, Effect of Ni, Zn, Au, Sb and In on the suppression of the Cu_3Sn phase in Sn-10 wt.%Cu alloys, *J. Electron. Mater.* 50 (3) (2021) 881–892.

- [10] T. Laurila, J. Hurtig, V. Vuorinen, J.K. Kivilahti, Effect of Ag, Fe, Au and Ni on the growth kinetics of Sn-Cu intermetallic compound layers, *Microelectron. Reliab.* 49 (3) (2009) 242–247.
- [11] A. Yang, et al., Effect of indium on microstructure, mechanical properties, phase stability and atomic diffusion of Sn-0.7Cu solder: experiments and first-principles calculations, *Mater. Sci. Eng., A* 855 (2022).
- [12] F. Emadi, V. Vuorinen, H. Dong, G. Ross, M. Paulasto-Kröckel, Investigation of the microstructural evolution and detachment of Co in contact with Cu-Sn electroplated silicon chips during solid-liquid interdiffusion bonding, *J. Alloys Compd.* 890 (2022).
- [13] F. Emadi, V. Vuorinen, S. Mertin, K. Widell, M. Paulasto-Kröckel, Microstructural and mechanical characterization of Cu/Sn SLID bonding utilizing Co as contact metallization layer, *J. Alloys Compd.* 929 (2022), 167228.
- [14] F. Emadi, V. Vuorinen, M. Paulasto-Kröckel, Utilizing Co as a contact metallization for wafer-level Cu-Sn-In SLID bonding used in MEMS and MOEMS packaging, in: 2022 IEEE 9th Electron. Syst. Technol. Conf. ESTC 2022 - Proc., 2022, pp. 359–363.
- [15] O. Golim, et al., Achieving low-temperature wafer level bonding with Cu-Sn-In ternary at 150 °C, *Scripta Mater.* 222 (2023).
- [16] F. Emadi, S. Liu, A. Klami, N. Tiwary, V. Vuorinen, M. Paulasto-Kröckel, Low-temperature die attach for power components: Cu-Sn-In solid-liquid interdiffusion bonding, *ASDAM 2022 - Proc. 14th Int. Conf. Adv. Semicond. Devices Microsystems* (2022) 23–26, no. October.
- [17] H. Jun, et al., Anomalous multiple pop-in behavior in Cu-Sn-based intermetallic compounds during nanoindentation, *Mater. Sci. Eng., A* 612 (2014) 192–196.
- [18] J. Feng, C. Hang, Y. Tian, C. Wang, B. Liu, Effect of electric current on grain orientation and mechanical properties of Cu-Sn intermetallic compounds joints, *J. Alloys Compd.* 753 (Jul. 2018) 203–211.
- [19] D. Mu, H. Yasuda, H. Huang, K. Nogita, Growth orientations and mechanical properties of Cu 6Sn 5 and (Cu,Ni) 6Sn 5 on poly-crystalline Cu, *J. Alloys Compd.* 536 (2012) 38–46.
- [20] Z. Yin, F. Sun, M. Guo, Investigation of elevated temperature mechanical properties of intermetallic compounds in the Cu-Sn system using nanoindentation, *J. Electron. Packag.* Trans. ASME 142 (2) (Jun. 2020).
- [21] J.J. Yu, J.Y. Wu, L.J. Yu, H.W. Yang, C.R. Kao, Micromechanical behavior of single-crystalline Cu₆Sn₅ by picoindentation, *J. Mater. Sci.* 52 (12) (2017) 7166–7174.
- [22] D. Mu, H. Huang, S.D. McDonald, J. Read, K. Nogita, Investigating the mechanical properties, creep and crack pattern of Cu₆Sn₅ and (Cu,Ni)₆Sn₅ on diverse crystal planes, *Mater. Sci. Eng.* 566 (2013) 126–133.
- [23] J.M. Song, B.R. Huang, C.Y. Liu, Y.S. Lai, Y.T. Chiu, T.W. Huang, Nanomechanical responses of intermetallic phase at the solder joint interface - crystal orientation and metallurgical effects, *Mater. Sci. Eng.* 534 (2012) 53–59.
- [24] D. Mu, H. Huang, K. Nogita, Anisotropic mechanical properties of Cu₆Sn₅ and (Cu, Ni)₆Sn₅, *Mater. Lett.* 86 (2012) 46–49.
- [25] V. Kumar, Z.Z. Fang, J. Liang, N. Dariavach, Microstructural analysis of lead-free solder alloys, *Metall. Mater. Trans. A Phys. Metall. Mater. Sci.* 37 (8) (2006) 2505–2514.
- [26] Y. Tian, R. Zhang, C. Hang, L. Niu, C. Wang, Relationship between morphologies and orientations of Cu₆Sn 5 grains in Sn_{3.0}Ag_{0.5}Cu solder joints on different Cu pads, *Mater. Char.* 88 (2014) 58–68.
- [27] J.W. Xian, G. Zeng, S.A. Belyakov, Q. Gu, K. Nogita, C.M. Gourlay, Anisotropic thermal expansion of Ni₃Sn₄, Ag₃Sn, Cu₃Sn, Cu₆Sn₅ and βSn, *Intermetallics* 91 (2017) 50–64.
- [28] Y.V. Milman, B.A. Galanov, S.I. Chugunova, Plasticity characteristic obtained through hardness measurement, *Acta Met. mater.* 41 (9) (1993) 2523–2532.
- [29] F.X. Che, J.H.L. Pang, Characterization of IMC layer and its effect on thermomechanical fatigue life of Sn-3.8Ag-0.7Cu solder joints, *J. Alloys Compd.* 541 (2012) 6–13.
- [30] V.M.F. Marques, C. Johnston, P.S. Grant, Nanomechanical characterization of Sn-Ag-Cu/Cu joints - Part 1: Young's modulus, hardness and deformation mechanisms as a function of temperature, *Acta Mater.* 61 (7) (2013) 2460–2470.
- [31] D. Mu, H. Huang, K. Nogita, Anisotropic mechanical properties of Cu 6Sn 5 and (Cu,Ni) 6Sn 5, *Mater. Lett.* 86 (2012) 46–49.
- [32] H. Xu, et al., Wafer-level SLID bonding for MEMS encapsulation, *Adv. Manuf.* 1 (2013) 226–235.
- [33] S.K. Lin, T.Y. Chung, S.W. Chen, C.H. Chang, 250 °C isothermal section of ternary Sn-In-Cu phase equilibria, *J. Mater. Res.* 24 (8) (2009) 2628–2637.
- [34] Y.C. Wang, C.J. Fleshman, R.W. Song, S.Y. Tsai, J.G. Duh, Diversifying grain orientation and expediting 10 μm Cu/Sn/Cu TLP bonding process with Ni doping, *J. Mater. Sci. Mater. Electron.* 32 (2) (2021) 2639–2646.
- [35] Z.Y. Wu, T.C. Wang, Y.C. Wang, R.W. Song, S.Y. Tsai, J.G. Duh, Enhancing mechanical properties via adding Ni and Zn in Cu/Sn_{3.5}Ag/Cu transient liquid phase bonding for advanced electronic packaging, *J. Mater. Sci. Mater. Electron.* 33 (6) (2022) 3016–3023.
- [36] R.W. Song, W.Y. Chen, Y.C. Wang, Z.Y. Wu, S.Y. Tsai, J.G. Duh, Enhancing mechanical strength of full intermetallic microbump via grain refinement by Zn in thermocompression bonding, *Mater. Chem. Phys.* 291 (2022).
- [37] Y.M. Leong, A.S.M.A. Haseeb, H. Nishikawa, O. Mokhtari, Microstructure and mechanical properties of Sn–1.0Ag–0.5Cu solder with minor Zn additions, *J. Mater. Sci. Mater. Electron.* 30 (13) (2019) 11914–11922.
- [38] P.-W. Huang, et al., Microstructure and mechanical strength of Cu/Sn/Cu microbump via Ni and Zn doping into Cu substrate, *Mater. Chem. Phys.* (2023), 127392.
- [39] Y.L. Tseng, Y.C. Chang, C.C. Chen, Co effects upon intermetallics growth kinetics in Sn-Cu-Co/Ni and Sn-Cu-Co/Cu couples, *J. Electron. Mater.* 44 (1) (2015) 581–589.
- [40] C. chi Chen, Y. lun Tseng, Cross-interaction in Cu/Sn/Co/Sn/Ni and Cu/Sn-Co/Co/Sn-Co/Ni couples, *J. Electron. Mater.* 44 (3) (2015) 1021–1027.
- [41] X.F. Tan, S. Tao, L. Ran, R. Knibbe, K. Nogita, Cobalt-doped Cu₆Sn₅ Lithium-Ion Battery Anodes with Enhanced Electrochemical Properties, 2022, pp. 1264–1276.
- [42] W.A. Sasangka, C.L. Gan, D. Lai, C.S. Tan, C.V. Thompson, Characterization of the Young's modulus, residual stress and fracture strength of Cu-Sn-In thin films using combinatorial deposition and micro-cantilevers, *J. Micromech. Microeng.* 25 (3) (2015).
- [43] W. Huang, K. Pan, J. Zhang, Y. Gong, Effect of in-doping on mechanical properties of Cu₆Sn₅-based intermetallic compounds: a first-principles study, *J. Electron. Mater.* 50 (7) (2021) 4164–4171.
- [44] A. Luktuke, A.S.S. Singaravelu, A. Mannodi-Kanakkithodi, N. Chawla, Influence of Indium addition on microstructural and mechanical behavior of Sn solder alloys: experiments and first principles calculations, *Acta Mater.* 249 (2023).
- [45] F. Emadi, V. Vuorinen, H. Dong, G. Ross, M. Paulasto-Kröckel, Investigation of the microstructural evolution and detachment of Co in contact with Cu-Sn electroplated silicon chips during solid-liquid interdiffusion bonding, *J. Alloys Compd.* 890 (2022), 161852.
- [46] K. Fisher, *Fundamental of Solidification*, 1989.
- [47] Y. Wang, Y. Dong, X. Zhao, Y. Huo, Y. Liu, A first-principles computation-driven mechanism study on the solders dilute doping effects to η'-Cu₆Sn₅ growth kinetics, *J. Mater. Sci.* 56 (16) (2021) 9741–9753.
- [48] K. Nogita, et al., Kinetics of the η-η' transformation in Cu₆Sn₅.pdf, *Scripta Mater.* 65 (2011) 922–925.
- [49] S.F. Choudhury, L. Ladani, Grain growth orientation and anisotropy in Cu₆Sn₅ intermetallic: nanoindentation and electron backscatter diffraction analysis, *J. Electron. Mater.* 43 (4) (2014) 996–1004.
- [50] R.R. Chromik, R.P. Vinci, S.L. Allen, M.R. Notis, Nanoindentation measurements on Cu-Sn and Ag-Sn intermetallics formed in Pb-free solder joints, *J. Mater. Res.* 18 (9) (2003) 2251–2261.
- [51] X. Deng, M. Koopman, N. Chawla, K.K. Chawla, Young's modulus of (Cu, Ag)-Sn intermetallics measured by nanoindentation, *Mater. Sci. Eng., A* 364 (1–2) (2004) 240–243.
- [52] X. Deng, N. Chawla, K.K. Chawla, M. Koopman, Deformation behavior of (Cu, Ag)-Sn intermetallics by nanoindentation, *Acta Mater.* 52 (14) (2004) 4291–4303.
- [53] H. Tsukamoto, Z. Dong, H. Huang, T. Nishimura, K. Nogita, Nanoindentation characterization of intermetallic compounds formed between Sn-Cu (-Ni) ball grid arrays and Cu substrates, *Mater. Sci. Eng. B Solid-State Mater. Adv. Technol.* 164 (1) (2009) 44–50.
- [54] S.W. Fu, C.Y. Yu, T.K. Lee, K.C. Liu, J.G. Duh, Impact crack propagation through the dual-phased (Cu,Ni) 6Sn 5 layer in Sn-Ag-Cu/Ni solder joints, *Mater. Lett.* 80 (101) (2012) 103–105.
- [55] W.H. Chen, C.F. Yu, H.C. Cheng, S.T. Lu, Crystal size and direction dependence of the elastic properties of Cu 3Sn through molecular dynamics simulation and nanoindentation testing, *Microelectron. Reliab.* 52 (8) (2012) 1699–1710.
- [56] W. Huang, K. Pan, B. Wang, Y. Gong, Grain size effects on mechanical properties of nanocrystalline Cu₆Sn₅ investigated using molecular dynamics simulation, *Materials* 15 (11) (2022) 1–10.
- [57] S.N. Naik, S.M. Walley, The Hall-Petch and inverse Hall-Petch relations and the hardness of nanocrystalline metals, *J. Mater. Sci.* 55 (7) (2020) 2661–2681.
- [58] D. Mu, H. Huang, S.D. McDonald, K. Nogita, Creep and mechanical properties of Cu₆Sn₅ and (Cu,Ni)₆Sn₅ at elevated temperatures, *J. Electron. Mater.* 42 (2) (2013) 304–311.